# Drying ripe mango slices using step-down temperature far-infrared-hot air techniques

Suwit Paengkanya[1], Sutinon Patcharatvirakul[1], Ponlakrit Kumklam[2*]

(1. *Sustainable Industrial Management Engineering, Faculty of Engineering, Rajamangala University of Technology Phra Nakhon, Bangkok 10800, Thailand*;
2. *Industrial Materials Science, Faculty of Science and Technology, Rajamangala University of Technology Phra Nakhon, Bangkok 10800, Thailand*)

**Abstract:** A key challenge in food drying is achieving an optimal balance between processing efficiency, energy consumption, and maintaining high quality in the final product. This study investigates three drying methods for mango slices: conventional hot air drying (HA), far-infrared combined hot air drying (FIRHA), and step-down temperature FIRHA. The effects of various operating parameters were analyzed, including drying medium temperature and the influence of far-infrared assistance, on the drying kinetics and quality attributes of the mango slices. The quality attributes assessed include color, shrinkage percentage, texture profile, water activity, microstructure, and energy consumption. The results indicate that the drying rates for FIRHA were significantly higher than those for HA. Mango slices dried using FIRHA and step-down temperature FIRHA exhibited greater lightness and greenness, along with increased crispness, while demonstrating lower yellowness compared to those dried by HA. The far-infrared assistance resulted in larger pore sizes and a higher void area fraction in the mango slices, but it also led to reduced hardness and shrinkage percentage compared to those dried using HA. In terms of specific energy consumption, the electric heater consumed significantly more energy than the far-infrared radiator and blower. Additionally, the total specific energy consumption of step-down temperature FIRHA was lower than that of both HA and FIRHA under all drying conditions. Based on these findings, this study recommends using step-down temperature FIRHA at 90°C for 1 h for the effective drying of mango slices, offering an optimal solution to the core challenges in the field. Ultimately, this work provides a valuable framework and empirical evidence for the adoption of hybrid drying technologies, contributing significantly to the fields of food engineering and sustainable agricultural processing.

**Keywords:** combined far-infrared-hot air drying, dried mango slices, drying kinetic, specific energy consumption, step-down temperature technique, texture

**DOI:** 10.25165/j.ijabe.20251806.9770

**Citation:** Paengkanya S, Patcharatvirakul S, Kumklam P. Drying ripe mango slices using step-down temperature far-infrared-hot air techniques. Int J Agric & Biol Eng, 2025; 18(6): 281–289.

## 1 Introduction

Nam Dok Mai mango is a popular tropical fruit in Thailand, known for its delicious taste, nutritional benefits, and potential economic value. The high demand for this fruit in international markets is evident from the significant contributions of dried mango products, which had an export value exceeding 37.4 million USD in 2023[1]. The popularity of dried mango can be attributed to its extended shelf life and convenience, making it a value-added product with considerable economic potential. HA drying is the most commonly used method in the food industry. It employs convective heat transfer to remove moisture, making it cost-effective and relatively easy to operate. However, HA drying has notable limitations. It requires prolonged drying times since its efficiency depends on surface evaporation, which becomes less effective as internal moisture diffusion slows during the later stages of drying. Additionally, heat loss to the environment decreases overall energy efficiency. Extended exposure to high temperatures can also degrade the sensory and nutritional quality of dried products, resulting in issues such as color darkening and texture hardening[2-4].

Far-infrared radiation (FIR) has emerged as an innovative drying technique, using a unique energy transfer mechanism that allows for direct absorption of energy by water molecules within the product[5]. FIR occupies the wavelength band of 3 to 1000 $\mu$m within the electromagnetic spectrum, and is used in thermal food processing applications such as heating, drying, and pasteurization. Thermal radiation spans wavelengths from 0.1 to 100 $\mu$m, encompassing parts of the ultraviolet spectrum, all visible light, and a portion of FIR. This radiation is emitted by all objects at temperatures above absolute zero. When thermal radiation interacts with a material's surface, its energy is divided based on the properties of that material: some energy is absorbed, some is reflected, and some is transmitted. The absorption of radiation in the thermal range, including FIR, excites molecular vibrations within the material, converting radiant energy directly into heat[6].

FIR minimizes thermal degradation, improving both energy efficiency and product quality. Compared to conventional methods, FIR significantly reduces drying time[7,8] and helps preserve bioactive compounds, maintain natural color, and prevent excessive

**Received date:** 2025-03-05 **Accepted date:** 2025-09-04

**Biographies: Suwit Paengkanya**, PhD, Assistant Professor, research interest: food engineering and drying technology, Email: suwit.p@rmutp.ac.th; **Sutinon Patcharatvirakul**, MEng, research interest: drying technology and engineering, Email: sutinon-pa@rmutp.ac.th.

***Corresponding author: Ponlakrit Kumklam**, PhD, Lecturer, research interest: agricultural engineering and drying technology. Industrial Materials Science, Faculty of Science and Technology, Rajamangala University of Technology Phra Nakhon, 1381 Pracharat 1 Road, Wongsawang, Bang Sue, Bangkok 10800, Thailand Tel: +66-2836-3000, Email: ponlakrit.k@rmutp.ac.th.

shrinkage[9]. The integration of FIR and HA, known as FIRHA drying, combines the rapid moisture removal benefits of FIR with the consistent heat transfer of HA. Research indicates that FIRHA can achieve higher head rice yield during paddy drying[10], superior texture retention in banana slices[11], accelerated storage of blueberries[12], and preservation of freshness with minimal nutritional loss in onions[13]. The drying kinetics of biological materials typically follow a characteristic pattern: an initial high drying rate due to surface moisture evaporation, followed by a declining rate as moisture from inner layers diffuses outward. This decline often leads to inefficiencies, particularly in conventional drying systems. Step-down temperature drying has been proposed to address these limitations by gradually reducing the drying temperature in stages, allowing for less heat input during later stages. This method prevents over-drying and maintains the textural and sensory properties of the product[14]. Combining FIRHA with step-down temperature drying presents a tailored solution by leveraging the rapid initial drying capability of FIR while also benefiting from the energy-efficiency and moisture redistribution enabled by step-down techniques. This innovative approach is supported by findings in other food products, such as improved rehydration ratios and reduced energy consumption[15], enhanced retention of bioactive compounds along with improved texture[16], and better color retention with reduced shrinkage in dried bananas[11].

The objective of this study is to evaluate the combined effect of FIRHA and step-down temperature drying on the drying kinetics, energy consumption, and quality attributes of Nam Dok Mai mangoes. The investigation will focus on critical quality parameters such as color, shrinkage, texture, and water activity, contributing to the optimization of drying technology for tropical fruits.

## 2 Material and methods

### 2.1 Experimental setup

The combined far-infrared radiation-hot air dryer (FIRHAD) is shown in Figure 1. Mango slices were dried using a tray dryer with dimensions of 30 cm×34 cm×50 cm. The drying chamber was equipped with a 1.2 kW electrical heater and a 650 W far-infrared radiator. Additionally, a backward-curved blade centrifugal fan, driven by a 0.09 kW motor, was included in the drying chamber, as shown in Figure 1. The samples were placed on a stainless-steel sieve tray. The drying air was heated by the electrical heater, which was controlled by proportional-integral-derivative (PID) controllers. The desired air velocity was controlled by a frequency inverter, which governed the rotation speed of the motor.

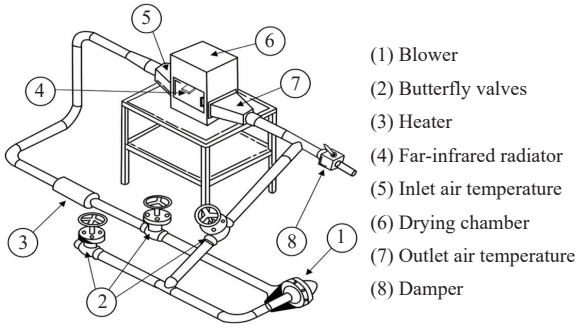


Figure 1 A schematic diagram of the FIRH

### 2.2 Material preparation

Ripe Nam Dok Mai mangoes were purchased from a local supermarket and allowed to ripen further at room temperature. The mangoes had a soluble solids content of approximately 18-19 °Brix, as measured by a refractometer (ATC, RHB-32/ATC, Thailand), with a mass ranging from 300-450 g. They were soaked in water at 47°C for 1.5 h to prevent enzymatic browning[17]. The initial moisture content of the mangoes ranged between 400% and 450% dry basis (d.b.). The moisture content of mangoes was determined by drying them in an oven (Memmert, Model UF75, Germany) at 103°C for 3 h, following a procedure similar to the standard method of the AOAC[18]. After peeling, the mangoes were sliced into pieces 1.5 cm thick using a knife.

### 2.3 Drying of mango slices

Before starting each drying experiment, the drying system was warmed up until the desired temperature was reached. The mango slices weighing 260±1 g were placed on a drying tray measuring 23 cm×27 cm and were dried under the conditions specified in Table 1, with a superficial air velocity of 0.5 m/s. The inlet air temperature was controlled by a PID type controller, maintaining an accuracy of ±1°C. The inlet and outlet air temperatures of the drying chamber were measured using k-type thermocouple with an accuracy of ±1°C, connected to a data logger (Yokogawa, Model FX1010, Japan). Initially, 20% of the drying air was recycled for the first 90 min, after which the recycle fraction was increased to 80% until the end of the process. The samples were dried until their final moisture content did not exceed 15% (d.b.). Samples were taken out of the dryer every 30 min to determine their moisture content using an electronic balance (A&D, Model FX-2000i, Japan) with a precision of ±0.01 gram. The surface temperature of the mangoes was measured with an infrared thermometer (BENETECH, Model GM320, China) accurate to ±1.5°C. The dried samples were then stored in a sealed aluminum bag and kept in a refrigerator at 4-6°C for 3 d to allow for moisture equilibration and hardness stabilization before further analysis. Each drying experiment was performed in triplicate.

**Table 1 Details of operating parameters for the drying tests**

| Test No. | Drying conditions |
|---|---|
| 1 | Hot air heating at 70°C (HA70°C) |
| 2 | Infrared heating combined with hot air heating at 70°C (FIRHA70°C) |
| 3 | Infrared heating combined with hot air heating at 80°C (FIRHA80°C) |
| 4 | Infrared heating combined with hot air heating at 90°C (FIRHA90°C) |
| 5 | Infrared heating combined with hot air heating at 100°C (FIRHA100°C) |
| 6 | FIRHA90°C for 1 h, then FIRHA80°C for 1 h, followed by FIRHA70°C until the end of the process (Step-down temperature FIRHA90°C for 1 h) |
| 7 | FIRHA90°C for 1.5 h, then FIRHA80°C for 1 h, followed by FIRHA70°C until the end of the process (Step-down temperature FIRHA90°C for 1.5 h) |
| 8 | FIRHA90°C for 2 h, then FIRHA80°C for 1 h, followed by FIRHA70°C until the end of the process (Step-down temperature FIRHA90°C for 2 h) |
| 9 | FIRHA 100°C for 1 h, then FIRHA80°C for 1 h, followed by FIRHA70°C until the end of the process (Step-down temperature FIRHA100°C for 1 h) |
| 10 | FIRHA 100°C for 1.5 h, then FIRHA80°C for 1 h, followed by FIRHA70°C until the end of the process (Step-down temperature FIRHA100°C for 1.5 h) |
| 11 | FIRHA 100°C for 2 h, then FIRHA80°C for 1 h, followed by FIRHA70°C until the end of the process (Step-down temperature FIRHA100°C for 2 h) |

### 2.4 Color measurement

The color of a mango slices sample was examined by a spectrophotometer (Konica Minolta, CM-3500d, Japan) with a D65 illuminant and an observer angle of 10°. The color was described using the CIE color system. Prior to each measurement, the spectrophotometer was calibrated with a standard white plate having standard value of $L^*$=93.19, $a^*$=1.12, and $b^*$=1.33, where $L^*$, $a^*$, and $b^*$ are the lightness/darkness, redness/greenness, and yellowness/blueness of the sample, respectively. Each color

measurement was performed at six different positions around the mango surface, and three samples were used.

### 2.5 Microstructure determination and image analysis

A scanning electron microscope (JEOL, JSM-5410LV, Tokyo, Japan) was used to study the microstructure of dried mango slices. To remove moisture from the dried samples, the mango pieces were sequentially immersed in 30% v/v alcohol for 1 h, followed by 50% v/v alcohol for 1 h, 70% v/v alcohol for 12 h, 95% v/v alcohol for 1 h, and finally 100% v/v alcohol for 1 h. The dried sample was cross-section intersected and placed on two-side adhesive tape attached to metal stubs and was coated with gold. SEM micrographs were taken at an accelerating voltage of 15 kV and a magnification of 150 times.

ImageJ software was used to analyze the images and calculate the porosity parameters of the dried mango slices based on pore size and pore area. The Otsu's method was implemented in this software to segment the solid phase and pores in a binary image. Pores were depicted as black, while the solid phase was represented by white. Subsequently, the diameter and pore area of the dried mango slices within the binary image were computed.

### 2.6 Shrinkage determination

The volumes of fresh and dried mango slices were measured using the volumetric displacement method with n-heptane, which has a density of 0.684 g/cm$^3$, as the working liquid. The percentage of shrinkage was calculated using the formula:

$$\text{Shrinkage} = \frac{(V_0 - V)}{V_0} \times 100\% \quad (1)$$

where, $V_0$ is the initial volume of the mango, m$^3$ and $V$ is the volume after drying, m$^3$. This measurement was conducted with ten replications to ensure accuracy.

### 2.7 Texture determination

The texture of dried mango slices was analyzed using a bench-top texture analyzer (Stable Micro Systems, model TA-XT, UK). Each sample was placed on a hollow planar base, and a direct force was applied using a 2 mm spherical probe. The pretest speed, test speed, and post-test speed of the probe were set at 1.5 mm/s, 2 mm/s, and 10 mm/s, respectively. Hardness was defined as the maximum force recorded on the force-deformation curve, while toughness was characterized by the area under the curve between the peak force and deformation. A total of ten samples were tested, and the average values were reported.

### 2.8 Water activity determination

The water activity of dried mango slices was measured using a water activity analyzer (Novasina Model Lab Master-aw, Switzerland) at 25°C. The dried mango slices were cut into small pieces and placed in containers. The analyzer analyzed 5 g of dried mango slices. In each experiment, the average of three water activity measurements was recorded.

### 2.9 Specific energy consumption

The energy efficiency was calculated based on the total energy used during the drying process relative to the total amount of evaporated moisture. This can be expressed with the following equation:

$$\text{SEC} = \frac{2.6(E_m + E_{\text{fir}}) + E_h}{M_w} \quad (2)$$

where, SEC is the specific energy consumption (MJ/kg evaporated water); $E_m$ is the electrical energy for driving the blower, MJ; $E_{\text{fir}}$ is the electrical energy for far-infrared radiator to penetrate and heat the samples, MJ; $E_h$ is the energy required for the electric heater to heat the ambient air to a desired temperature, MJ; and $M_w$ is the total amount of evaporated water, kg. It is important to note that the value of 2.6 is used as a conversion factor to translate electrical energy into primary energy. All electrical energy consumptions were measured directly with kilowatt-hour meters (DAI-ICHI, DD28, Thailand).

### 2.10 Statistical analysis

The data from the experiment, which included color, shrinkage, hardness, toughness, and water activity, were statistically analyzed using Analysis of Variance (ANOVA). The Duncan's New Multiple Range Test was employed to assess mean differences, utilizing the SPSS program (SPSS, Version 13). Average values of the quality data were considered at a 95% confidence interval.

## 3 Results and discussion

### 3.1 Drying kinetics of Nam Dok Mai mango

Figure 2 shows the drying kinetics of Nam Dok Mai mango via the FIRHA and HA drying. The results indicate that the moisture content reduction of the FIRHA drying decreased significantly faster than the HA drying. The decline in moisture content exhibited an exponential trend over time, a pattern commonly observed in food materials[19,20]. As shown in Figure 2, the FIRHA drying at drying air temperature of 90°C reduced the initial moisture content of 440% (d.b.) down to a final moisture content of 15% (d.b.) within 360 min, making it the fastest drying method compared to other conditions. This is because the temperature of mango slices during FIRHA drying was higher than during HA drying, resulting in a higher mass transfer rate[21]. When comparing drying conditions at a temperature of 70°C, the FIRHA method demonstrated a faster moisture reduction, decreasing between 3% and 30%. Furthermore, increasing the temperature from 70°C to 90°C enhanced the moisture reduction rate in FIRHA drying, resulting in a reduction of 32% to 66% over a drying time of 30 to 90 min. These findings confirm that the use of FIR could enhance the drying rate by allowing the inner moisture to absorb infrared energy, which serves as the driving force for increased moisture evaporation[3]. During FIRHA heating, radiation from the source interacted with the product. A portion of this radiation was absorbed, while the rest was either reflected or passed through. The absorbed radiation penetrated, primarily inducing vibrations in water molecules. This process generated heat quickly and throughout the material, warming both the surface and the internal layers simultaneously. As internal heat built up, it increased the temperature of the food and the vapor pressure of its internal moisture. This elevated vapor pressure drove moisture toward the cooler surface. Concurrent hot air flow over the surface then evaporated this moisture, lowering the surface temperature. This temperature gradient further promoted the movement of internal moisture toward the surface[22].

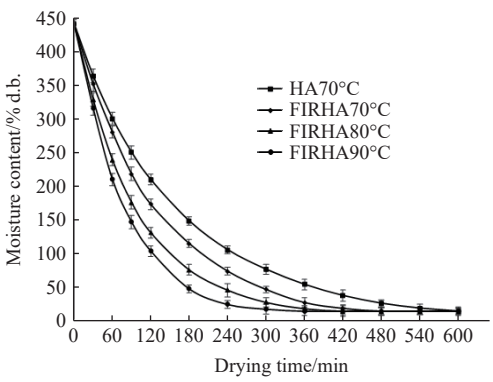


Figure 2 Changes in the moisture content of mango slices during FIRHA and HA drying

Figure 3 shows the reduction of moisture content during step-down temperature FIRHA drying. The results indicated that increasing the drying air temperature in step-down FIRHA drying led to a significantly faster decrease in the moisture content of mango slices. As shown in Figure 3, the moisture content reduction of step-down temperature of FIRHA100°C for 1 h was faster decreased than the step-down temperature of FIRHA90°C for 1 h around 55%. The higher drying air temperature during the initial stage of step-down temperature of FIRHA drying resulted in more rapid moisture reduction. This phenomenon occurs because a higher drying air temperature creates a larger difference between the drying temperature and the material's surface temperature, thereby increasing the evaporation rate of moisture from the surface[22].

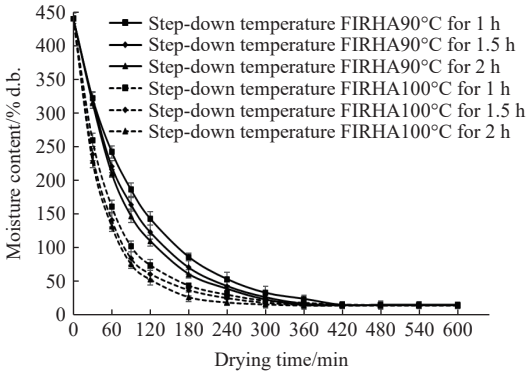


Figure 3 Changes in the moisture content of mango slices during step-down temperature FIRHA drying

Additionally, a higher drying air temperature combined with a longer drying time generally resulted in greater moisture content reduction, as expected. The step-down temperature of FIRHA100°C for 2 h was provided a faster moisture reduction compared with the drying condition of step-down temperature of FIRHA90°C for 2 h in the range of 4%-55%. Conversely, the moisture content reduction at the same drying air temperature did not show significant differences during the first 210 min. This suggests that the drying temperature during the initial stage of step-down temperature FIRHA drying has a more substantial impact on moisture reduction. The variations in moisture reduction levels, as shown in Figure 3, were clearly noticeable.

Figures 4-6 show the changes in inlet air temperature ($T_{in}$), outlet air temperature ($T_{out}$), and the temperature of mango slices ($T_p$) under different drying conditions. In the case of hot air drying, with an inlet air temperature of 70°C, the outlet air temperature was approximately 4°C-6°C lower than the inlet temperature. During this process, the mango slices absorbed energy from the drying air, which allowed moisture from the inside to move to the surface and evaporate into the ambient air. In contrast, during FIRHA drying at a temperature of 90°C, the outlet air temperature was initially lower than the inlet temperature for the first 180 min. After this period, the outlet air temperature approached the inlet air temperature. This phenomenon can be explained by two factors. First, as drying time increased, the rate of moisture evaporation decreased, resulting in less energy being absorbed by the samples and subsequently increasing the outlet air temperature. Second, the combination of far-infrared and hot air drying contributed additional energy to the drying process, leading to a rise in the outlet temperature at the exit port. As shown in Figure 6, the product temperature experienced a rapid increase during the first 60 min of drying. After this initial period, the temperature rise slowed, indicating the onset of the falling rate period[23]. Notably, the temperature of the mango slices dried using FIRHA increased more rapidly than that of the slices dried using hot air alone. These results confirm that the mango slices were effectively absorbing energy from the far-infrared radiator. Additionally, high product temperatures affect the degradation of beta-carotene; therefore, it is important to be cautious when selecting the drying temperature to maintain the product's nutrients[24,25].

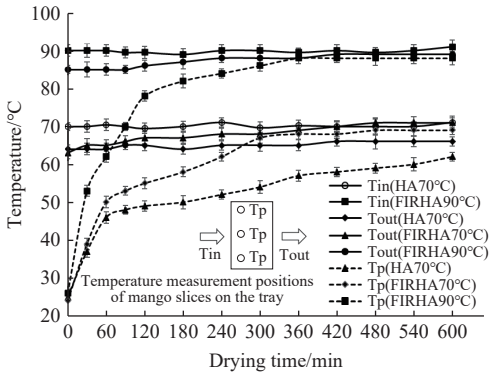


Figure 4 Changes in inlet and outlet air temperatures and mango slices temperature during FIRHA and HA drying

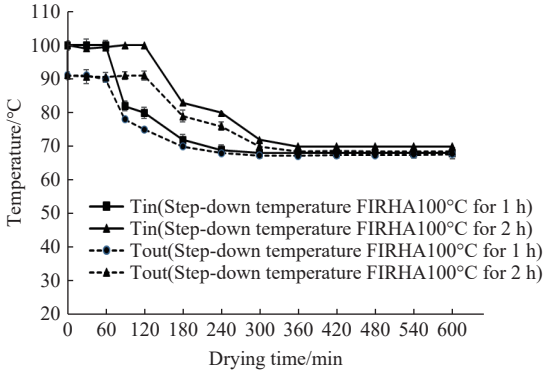


Figure 5 Changes in the inlet and outlet air temperatures during step-down temperature FIRHA at 100°C for 1 and 2 h

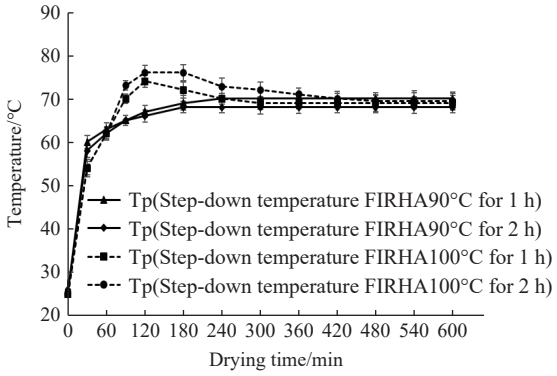


Figure 6 Changes in the mango slices temperature during drying using step-down temperature FIRHA drying at 90°C and 100°C for 1 and 2 h

Figure 5 shows the inlet and outlet air temperatures for drying mango slices using the step-down temperature FIRHA drying. At a step-down temperature FIRHA 100°C, the outlet air temperature at the exit of the drying chamber was approximately 10% lower than the inlet air temperature for the first 120 min. After this period, the outlet air temperature began to reach the inlet air temperature. During the drying time of 120-180 min, the outlet air temperature from both FIRHA and step-down temperature FIRHA drying increased to nearly match the inlet air temperature, indicating the

onset of the falling rate phase of drying[4,26,27]. Figure 6 shows the product temperature for the step-down temperature FIRHA drying. Initially, as the drying air temperature increased during the first stage, the product temperature was significantly higher between 90 and 180 min. Following this time frame, the product temperature decreased to nearly the outlet air temperature. These results are similar to those observed with the FIRHA and HA drying. Therefore, the step-down temperature FIRHA drying demonstrates a significant advantage in energy efficiency, which will be discussed in the specific energy consumption section.

### 3.2 Color of dried mango slices

Table 2 shows the color of dried mango slices under different drying conditions. The mango slices dried using the step-down temperature FIRHA method, with an initial drying air temperature of 90°C for 1 h, exhibited higher lightness ($L^*$) but lower redness (+$a^*$) and yellowness (+$b^*$) compared to the other drying conditions. The values for lightness, redness, and yellowness were 71.38, 61.62, and 13.58, respectively. This is attributed to the higher product temperature during the first stage of the drying process, which allowed the step-down temperature technique to minimize non-enzymatic browning reactions. In contrast, the samples dried at a constant temperature of 90°C showed lower lightness ($L^*$) but increased greenness (+$a^*$) and yellowness (+$b^*$). This is because the higher product temperature during the entire drying process accelerated non-enzymatic browning reactions, resulting in a browner color[28,29], as shown in Figure 7. An increase in hot air temperature and extended drying time during the first stage of the step-down temperature FIRHA method, as well as a rise in hot air temperature in the FIRHA method, decreased the lightness but increased the redness and yellowness of dried mango slices. This is because the increased product temperature accelerated non-enzymatic browning reactions[4,30,31]. Additionally, many research papers have found that the color of dried products and the drying temperature correlate with nutrients such as vitamin C content in jujube slices[32], ginsenoside in Panax notoginseng roots[33], and phenolic composition of chrysanthemum[34].

**Table 2 Colors of dried mango slices under different drying conditions**

| Drying conditions | $L^*$ | $a^*$ | $b^*$ |
|---|---|---|---|
| HA70°C | 63.29±1.78$^{bc}$ | 17.68±1.06$^{c}$ | 55.01±1.85$^{bc}$ |
| FIRHA70°C | 66.77±1.90$^{ef}$ | 15.11±0.53$^{a}$ | 56.19±1.72$^{cd}$ |
| FIRHA80°C | 63.46±1.47$^{bc}$ | 18.58±1.26$^{cd}$ | 54.73±1.61$^{bc}$ |
| FIRHA90°C | 54.26±1.82$^{a}$ | 19.34±1.38$^{d}$ | 48.66±1.92$^{a}$ |
| Step-down temperature FIRHA90°C for 1 h | 71.38±1.97$^{g}$ | 13.58±1.10$^{a}$ | 61.62±1.97$^{f}$ |
| Step-down temperature FIRHA90°C for 1.5 h | 68.25±1.78$^{f}$ | 14.63±1.82$^{ab}$ | 59.91±1.80$^{e}$ |
| Step-down temperature FIRHA90°C for 2 h | 64.48±1.93$^{cd}$ | 15.41±1.08$^{b}$ | 55.97±1.93$^{cd}$ |
| Step-down temperature FIRHA100°C for 1 h | 67.34±1.57$^{f}$ | 14.81±1.05$^{b}$ | 56.91±1.51$^{d}$ |
| Step-down temperature FIRHA100°C for 1.5 h | 65.47±1.75$^{de}$ | 15.28±0.89$^{b}$ | 56.13±1.97$^{cd}$ |
| Step-down temperature FIRHA100°C for 2 h | 62.06±1.89$^{b}$ | 18.79±1.48$^{cd}$ | 54.08±1.75$^{b}$ |

Note: Different superscript letters in the same column indicate statistical difference ($p$<0.05).

### 3.3 Microstructure and pore size distribution of dried mango slices

Figure 8 shows the microstructure of dried mango slices processed through different drying techniques. It was observed that the pore size of the dried mango slices increased with elevated drying temperatures. The samples dried using FIRHA70°C drying exhibited larger pore sizes compared to those dried with conventional HA drying. This finding supports the idea that far-infrared radiation penetrates the samples, enhancing moisture transfer from the inner layers to the outer surface[35]. In the initial

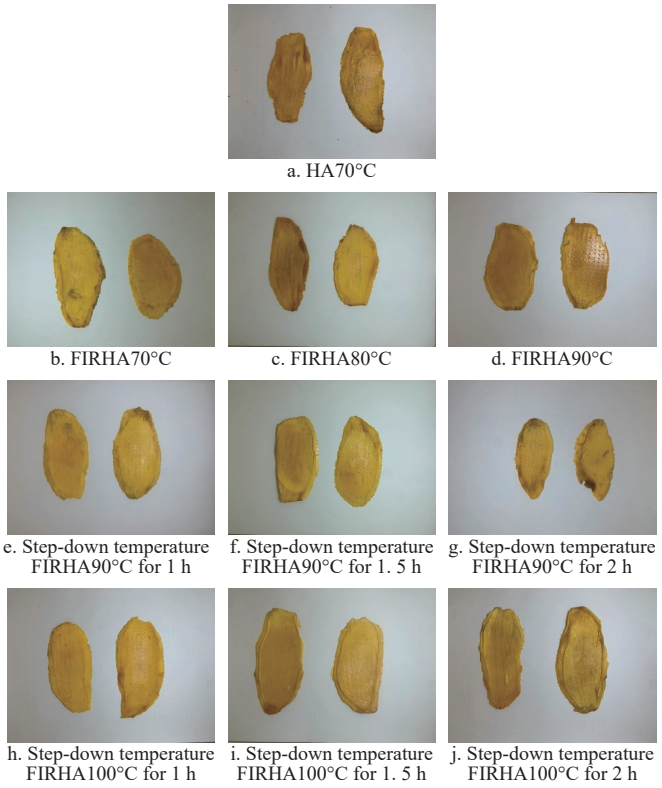


Figure 7 Colors of dried mangoes under various drying conditions

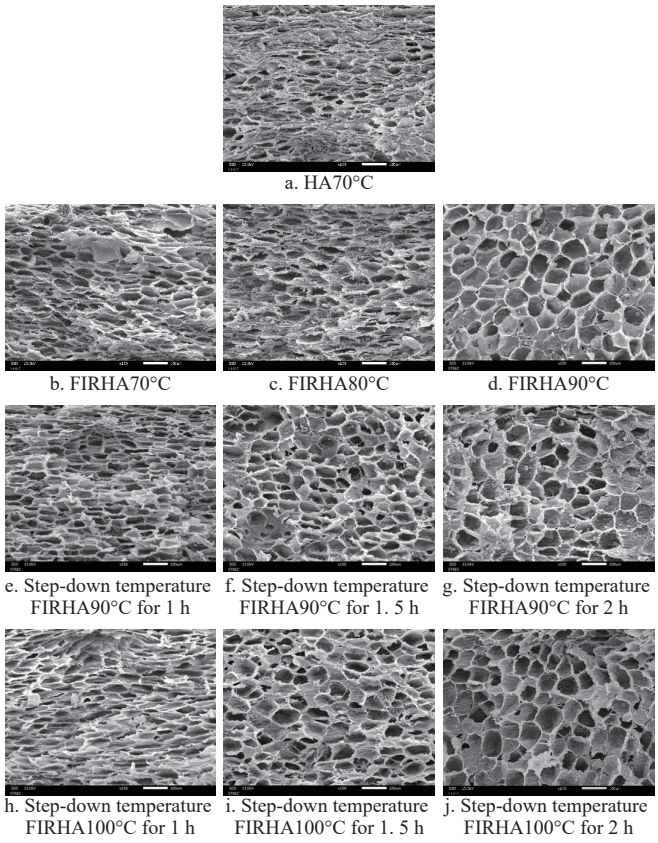


Figure 8 Cross-sectional microstructures and binary images of dried mango slices under various drying conditions

stages of step-down temperature FIRHA drying, the elevated drying temperatures contributed to the development of a more porous structure. As shown in Figure 8, the high temperature during drying led to rapid moisture evaporation from inside the samples, creating high vapor pressure, which in turn formed a porous structure[36]. Therefore, the higher temperatures used in FIRHA drying resulted in larger pore sizes.

Figure 9 shows the pore size and void area fraction inside the microstructure of the dried mango slices using various drying techniques. The results showed that the mango slices dried using the FIRHA and step-down temperature FIRHA techniques had more pores with diameters between 70 and 120 $\mu$m and a higher void area fraction than those dried with the HA method. However, the void area fraction of mango slices dried using the HA method was

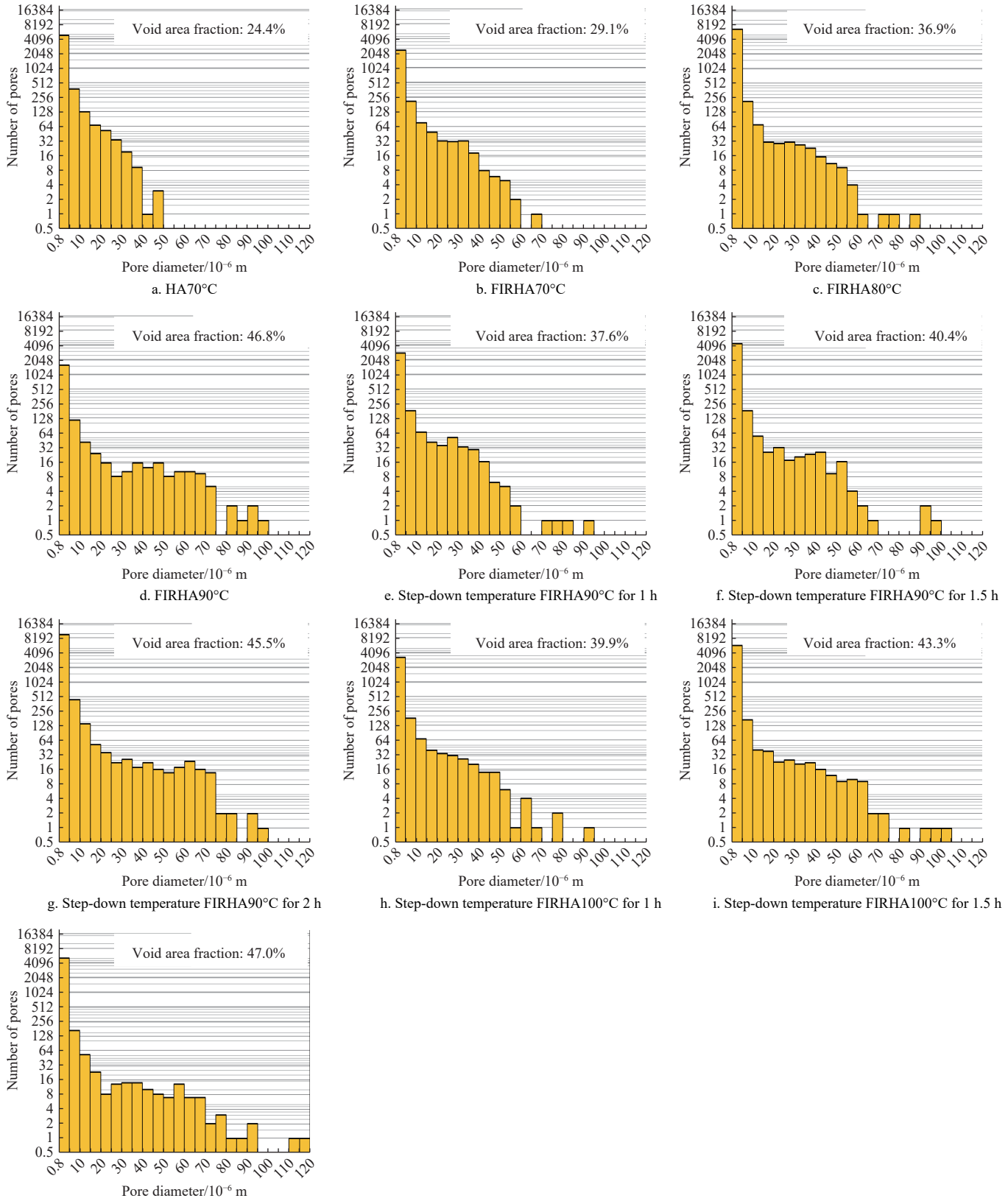


a. HA70°C
b. FIRHA70°C
c. FIRHA80°C
d. FIRHA90°C
e. Step-down temperature FIRHA90°C for 1 h
f. Step-down temperature FIRHA90°C for 1.5 h
g. Step-down temperature FIRHA90°C for 2 h
h. Step-down temperature FIRHA100°C for 1 h
i. Step-down temperature FIRHA100°C for 1.5 h
j. Step-down temperature FIRHA100°C for 2 h

Figure 9 Pore size distributions of dried mango slices under various drying conditions

24.4%, and the pore size was less than 50 $\mu$m, as shown in Figure 9a. This discrepancy is explained by the internal vapor pressure that is produced in the dried samples during FIRHA and step-down temperature FIRHA drying, which causes the water to evaporate quickly and the tissue to expand as a result. The initial drying temperature and duration during the first stage of step-down temperature FIRHA drying significantly influenced the pore size and void area fraction of the dried mango slices. As demonstrated in Figure 9, higher temperatures and longer first-stage drying times resulted in larger pore sizes and greater void area fractions. Similarly, higher hot air temperatures in the FIRHA drying process also resulted in larger pore sizes and greater void area fractions in the dried samples.

### 3.4 Shrinkage percentages of dried mango slices

The shrinkage percentages of the mango slices are presented in Table 3. The results indicate that the shrinkage percentages of the samples ranged from 70.73% to 84.44%. The mango slices dried using HA drying exhibited the highest shrinkage percentages. This was attributed to the longer drying time, which led to smaller pores in the mango pulp[3]. When far-infrared drying was combined with hot air drying, the shrinkage percentages decreased. Specifically, at a drying air temperature of 70°C, the shrinkage percentage for FIRHA drying decreased by 4.18% compared to HA drying alone. This reduction is due to the ability of far-infrared to penetrate the inner pulp of the mangoes, facilitating moisture transfer from the inner to the outer surface of the samples The pressure in the pores helps stabilize the samples. As the drying temperature of FIRHA drying increased from 70°C to 90°C, the shrinkage percentages decreased by approximately 10%. The higher hot air temperature enhanced moisture evaporation and reduced drying time, resulting in less shrinkage. The results from increased drying temperature during step-down temperature FIRHA drying showed similar outcomes to FIRHA drying. These findings confirm that far-infrared can penetrate the inner pulp, creating larger pore sizes and contributing to the stability of the samples[4,37-39]. Furthermore, many research papers claim that the relative humidity of drying air affects the product structure, which predominantly influences the shrinkage percentages. They found that a step-down in relative humidity during drying significantly reduces volume shrinkage[27,35].

**Table 3 Shrinkage percentages of dried mango slices under different drying conditions**

| Drying conditions | Shrinkage/% | Drying time/min |
|---|---|---|
| HA70°C | 84.44±1.92$^{f}$ | 600 |
| FIRHA70°C | 80.26±2.59$^{e}$ | 480 |
| FIRHA80°C | 78.46±2.28$^{de}$ | 360 |
| FIRHA90°C | 69.97±1.90$^{a}$ | 252 |
| Step-down temperature FIRHA90°C for 1 h | 76.89±2.36$^{d}$ | 414 |
| Step-down temperature FIRHA90°C for 1.5 h | 74.10±2.29$^{c}$ | 402 |
| Step-down temperature FIRHA90°C for 2 h | 73.50±2.38$^{bc}$ | 390 |
| Step-down temperature FIRHA100°C for 1 h | 73.59±2.17$^{bc}$ | 408 |
| Step-down temperature FIRHA100°C for 1.5 h | 71.37±2.38$^{abc}$ | 384 |
| Step-down temperature FIRHA100°C for 2 h | 70.73±2.28$^{ab}$ | 360 |

Note: Different superscript letters in the same column indicate statistical difference ($p < 0.05$).

### 3.5 Texture profile and water activity of dried mango slices

The texture profile and water activity of dried mango slices under different drying conditions are shown in Table 4. The hardness and toughness of the mango slices were evaluated as part of the texture analysis. Hardness was measured based on the maximum peak of the breaking force, while toughness represents a material's ability to absorb energy before fracturing, measured in terms of the force applied over the collapse distance of the samples. The results indicated that the hardness values of the samples ranged from 6.37 to 13.97 N, while toughness values ranged from 6.55 to 13.25 N·mm. Samples dried using the FIRHA drying and the step-down temperature FIRHA drying exhibited lower hardness values compared to those dried with HA drying. The higher drying air temperature during the first stage of the step-down temperature FIRHA drying process contributed to this reduced hardness. Specifically, as the drying air temperature increased by 10% in the first stage of step-down temperature FIRHA drying, the hardness decreased by 1.27 to 2.23 N. Additionally, the hardness of the samples dried using FIRHA was lower with increasing drying air temperature, consistent with the hardness values observed in step-down temperature FIRHA drying. The toughness values for the mango slices displayed a similar trend to the hardness values across the different drying conditions. The lowest toughness value recorded was 6.26 N·mm at a drying condition of FIRHA with a drying air temperature of 90°C. While drying at higher temperatures provided the advantage of a crisper texture, it also increased the possibility of catalysis of a non-enzymatic browning[29,35].

**Table 4 Texture profile and water activity of dried mango slices under different drying conditions**

| Drying conditions | Hardness/N | Toughness/ N·mm | Water activity |
|---|---|---|---|
| HA70°C | 13.79±2.23$^{e}$ | 13.25±2.43$^{d}$ | 0.571±0.010$^{b}$ |
| FIRHA70°C | 13.30±1.53$^{de}$ | 10.45±2.38$^{bc}$ | 0.534±0.010$^{a}$ |
| FIRHA80°C | 13.19±2.44$^{de}$ | 11.11±2.09$^{c}$ | 0.578±0.007$^{b}$ |
| FIRHA90°C | 6.37±2.01$^{a}$ | 6.26±2.16$^{a}$ | 0.573±0.010$^{b}$ |
| Step-down temperature FIRHA90°C for 1 h | 11.89±2.44$^{cd}$ | 9.58±2.22$^{bc}$ | 0.539±0.007$^{a}$ |
| Step-down temperature FIRHA90°C for 1.5 h | 11.57±1.47$^{bcd}$ | 9.82±2.41$^{bc}$ | 0.534±0.010$^{a}$ |
| Step-down temperature FIRHA90°C for 2 h | 11.15±2.27$^{cd}$ | 8.81±2.03$^{b}$ | 0.565±0.003$^{b}$ |
| Step-down temperature FIRHA100°C for 1 h | 11.95±2.53$^{cd}$ | 10.69±1.82$^{c}$ | 0.537±0.002$^{a}$ |
| Step-down temperature FIRHA100°C for 1.5 h | 10.24±2.26$^{bc}$ | 6.89±2.29$^{a}$ | 0.531±0.002$^{a}$ |
| Step-down temperature FIRHA100°C for 2 h | 9.88±2.48$^{b}$ | 6.55±1.87$^{a}$ | 0.538±0.004$^{a}$ |

Note: Different superscript letters in the same column indicate statistical difference ($p < 0.05$).

### 3.6 Specific energy consumption

The energy consumption of the drying process was evaluated in terms of specific energy consumption (SEC). The SEC includes both thermal and electrical energy. The specific thermal energy consumption ($SEC_{Thermal}$) was calculated based on the energy usage of the heater, while the specific electrical energy consumption ($SEC_{Electrical}$) was derived from the energy consumption of the far-infrared radiator and blower.

Figure 10 shows the specific energy consumption of the far-infrared radiator, heater, and blower under various operating conditions. The specific energy consumption of the far-infrared radiator and blower is significantly lower, approximately five to ten times less than that of the heater, depending on the drying conditions. This pattern is common in most drying systems. In these systems, ambient air is heated by the electric heater to generate hot air before it enters the drying process, which accounts for a substantial portion of the energy used for water evaporation[40]. Figure 11 shows the $SEC_{heater}$, $SEC_{electricity}$, total specific energy consumption ($SEC_{total}$), and drying time under different drying conditions. The $SEC_{heater}$ tends to increase with higher hot air

temperatures. A step-down temperature FIRHA90°C for 1-2 h of drying resulted in lower $SEC_{heater}$ values. The $SEC_{total}$ is directly related to $SEC_{heater}$, $SEC_{electricity}$, and the drying time. While increasing the drying temperature can reduce drying time, it also leads to greater energy consumption. For energy savings, a step-down temperature FIRHA90°C for 1 h is recommended for drying mango slices. In addition, if the goal is to minimize drying time, a step-down temperature FIRHA100°C for 2 h is preferable. However, when selecting drying conditions, it is essential to consider both the quality of the mango slices after drying and the associated energy consumption.

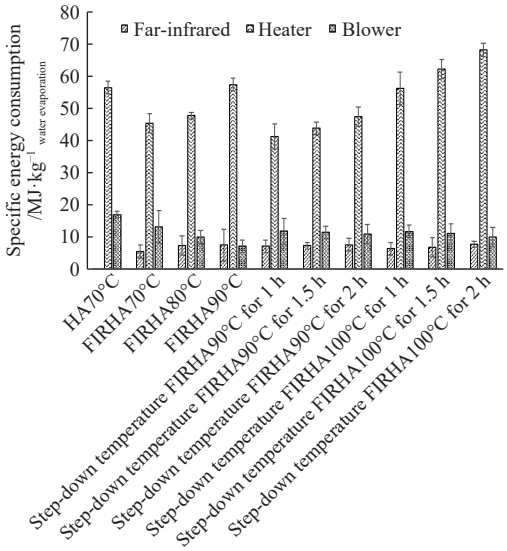


Figure 10 Specific energy consumption of drying process under different drying conditions

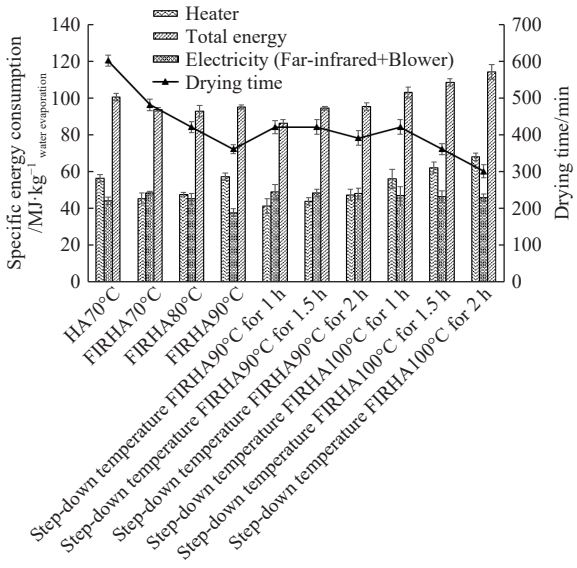


Figure 11 Specific energy consumption of drying process and drying times under different drying conditions

When considering the perspective of entrepreneurs in the drying industry, the specifics of a drying operation using the step-down temperature FIRHA at 90°C for 1 h can be examined. The SEC for this process was measured at 86.06 MJ/kg $_{water\ evaporated}$, or 23.9 kW·h/kg $_{water\ evaporated}$. In Thailand, the cost of electricity is approximately 0.12 USD/kW·h, resulting in an operation cost of 2.86 USD/kg $_{water\ evaporated}$. This cost is significantly higher compared to other drying systems. For instance, Soponronarit and Prachayawarakorn[41] conducted a feasibility study on paddy drying using a fluidization technique that reduced paddy moisture content from 38% to 25% (dry basis), reporting a lowest SEC of around 6 MJ/kg $_{water\ evaporated}$ and a cost of 0.08 USD/kg $_{water\ evaporated}$. While the mango drying system is indeed more expensive, it is important to consider the final product prices. Dried mango products, such as mango snacks, mango foam mats, and mango slices, are valued more highly than dried paddy. The unique flavors and appearance of Nam Dok Mai mango highlight its premium market appeal.

Additionally, scaling up the dryer from laboratory to pilot scale can reduce unit costs and the break-even point. Generally, dimensional analysis is utilized for scaling up dryer operations. Kitron and Tamir[42] successfully scaled up dryer from small to large scale, increasing the reactor volume three times, which in turn raised the heat transfer coefficient from 100 to 800 W/(m²·K). In the current work, the FIRHA dryer could also be scaled up using dimensional analysis or computer simulation techniques, which could be explored in future studies.

## 4 Conclusions

The reduction in moisture content when using FIRHA drying was significantly faster than with conventional HA drying. Increasing the drying air temperature during the step-down FIRHA drying resulted in a notably faster decrease in the moisture content of mango slices. The drying temperature during the initial stage of step-down FIRHA drying had a substantial impact on moisture reduction. Mango slices dried using the step-down temperature FIRHA method, with an initial drying air temperature of 90°C for 1 h, exhibited higher lightness and greenness, but lower yellowness compared to other drying conditions, with values of 71.38, 61.62, and 13.58, respectively. This outcome is attributed to the higher product temperature during the first stage of the drying process, which allowed the step-down temperature FIRHA technique to minimize non-enzymatic browning reactions. Additionally, the pore size of the dried mango slices increased with elevated drying temperatures. Samples dried at 70°C using FIRHA exhibited larger pore sizes and more void area fractions compared to those dried with conventional HA drying. The mango slices dried using HA drying showed the highest shrinkage percentages. Conversely, combining far-infrared drying with hot air drying resulted in decreased shrinkage percentages. FIRHA and step-down temperature FIRHA drying also exhibited lower hardness values compared to those dried with HA drying, primarily due to the higher drying air temperature during the initial stage of the step-down temperature FIRHA drying. The toughness values for the mango slices aligned closely with the hardness values across the various drying conditions. In terms of energy consumption, the specific energy consumption of the far-infrared radiator and blower is significantly lower, approximately five to ten times less than that of the heater. The total specific energy consumption is directly related to the specific energy consumption of heater, electricity, and the drying time. While increasing the drying temperature can reduce drying time, it also results in greater energy consumption. For energy efficiency, a step-down temperature of FIRHA90°C for 1 h is recommended for drying mango slices. To minimize drying time, a step-down temperature of FIRHA100°C for 2 h is preferable.

## Acknowledgements

The authors would like to thank the Faculty of Engineering and the Faculty of Science and Technology at Rajamangala University of Technology Phra Nakhon for their support in providing research tools and facilities.

## [References]


[1] Office of Agricultural Economics. Export statistics. 2023. https://impexpth.oae.go.th/export. Accessed on: [2024-12-10].

[2] Akpinar E K, Bicer Y. Mathematical modelling of thin layer drying process of long green pepper in solar dryer and under open sun. Energy Conversion and Management, 2008; 49(6): 1367–1375.

[3] Nathakaranakule A, Jaiboon P, Soponronnarit S. Far-infrared radiation assisted drying of longan fruit. Journal of Food Engineering, 2010; 100(4): 662–668.

[4] Nathakaranakule A, Paengkanya S, Soponronnarit S. Durian chips drying using combined microwave techniques with step-down microwave power input. Food and Bioproducts Processing, 2019; 116: 105–117.

[5] Chang A T, Zheng X, Xiao H W, Yao X D, Liu D C, Li X Y, et al. Short and medium-wave infrared drying of cantaloupe (*Cucumis melon* L.) slices: drying kinetics and process parameter optimization. Processes, 2022; 10: 114.

[6] Meseguer J, Pérez-Grande I, Sanz-Andrés A. Thermal radiation heat transfer. In: Meseguer J, Pérez-Grande I, Sanz-Andrés A, editors. Spacecraft Thermal Control. Woodhead Publishing. 2012; pp.73–86. doi: 10.1533/9780857096081.73.

[7] Xu B G, Zhang M, Bhandari B. Temperature and quality characteristics of infrared radiation–dried kelp at different peak wavelengths. Drying Technology, 2014; 32(4): 437–446.

[8] Huang D, Yang P, Tang X H, Luo L, Sunden B. Application of infrared radiation in the drying of food products. Trends in Food Science & Technology, 2021; 110: 765–777.

[9] Yao L Y, Fan L P, Duan Z H. Effect of different pretreatments followed by hot-air and far-infrared drying on the bioactive compounds, physicochemical property and microstructure of mango slices. Food Chemistry, 2020; 305: 125477.

[10] Meeso N, Nathakaranakule A, Madhiyanon T, Soponronnarit S. Influence of FIR irradiation on paddy moisture reduction and milling quality after fluidized bed drying. Journal of Food Engineering, 2004; 65(2): 293–301.

[11] Nimmol C, Devahastin S, Swasdisevi T, Soponronnarit S. Drying and heat transfer behavior of banana undergoing combined low-pressure superheated steam and far-infrared radiation drying. Applied Thermal Engineering, 2007; 27: 2483–2494.

[12] Liu Z L, Wang S Y, Huang X J, Zhang X H, Xie L, Bai J W, et al. Quality changes and shelf-life prediction of far-infrared radiation heating assisted pulsed vacuum dried blueberries by SSA-ELM. Food Chemistry, 2025; 473: 143060.

[13] Mongpraneet S, Abe T, Tsurusaki T. Accelerated drying of welsh onion by far infrared radiation under vacuum conditions. Journal of Food Engineering, 2002; 55(2): 147–156.

[14] Lekcharoenkul P, Tanongkankit Y, Chiewchan N, Devahastin S. Enhancement of sulforaphane content in cabbage outer leaves using hybrid drying technique and stepwise change of drying temperature. Journal of Food Engineering, 2014; 122: 56–61.

[15] Afzal T M, Abe T, Hikida Y. Energy and quality aspects during combined FIR-convection drying of barley. Journal of Food Engineering, 1999; 42(4): 177–182.

[16] Bassey E J, Cheng J H, Sun D W. Improving drying kinetics, physicochemical properties and bioactive compounds of red dragon fruit (Hylocereus species) by novel infrared drying. Food Chemistry, 2022; 375: 131886.

[17] Neamtang P, Nathakaranakule A, Paengkanya S, Thepa S, Soponronnarit S. Drying ripe mangoes using a step-down industrial microwave-hot air belt dryer. Drying Technology, 2024; 42: 2241–2255.

[18] AOAC. Official Methods of Analysis, 16th ed. Washington, DC: Association of Official Agricultural Chemists. 1995;1018p.

[19] Zhang W P, Pan Z L, Xiao H W, Zheng Z A, Chen C, Gao Z J. Pulsed vacuum drying (PVD) technology improves drying efficiency and quality of Poria cubes. Drying Technology, 2018; 36: 908–921.

[20] Amini G, Salehi F, Rasouli M. Color changes and drying kinetics modeling of basil seed mucilage during infrared drying process. Information Processing in Agriculture, 2022; 9(3): 397–405.

[21] Chen C, Liao C, Wongso I, Wang W B, Khir R, Huang G W, et al. Drying and disinfection of off-ground harvested almonds using step-down temperature hot air heating. LWT-Food Science and Technology, 2021; 152: 112282.

[22] El-Mesery H S, Mwithiga G. Performance of a convective, infrared and combined infrared-convective heated conveyor-belt dryer. Journal of Food Science and Technology, 2015; 52: 2721–2730.

[23] Chen C, Venkitasamy C, Zhang W P, Deng L Z, Meng X Y, Pan Z L. Effect of step-down temperature drying on energy consumption and product quality of walnuts. Journal of Food Engineering, 2020; 285: 110105.

[24] Pott I, Marx M, Neidhart S, Hlbauer W M, Carle R. Quantitative determination of , β-carotene stereoisomers in fresh, dried, and solar-dried mangoes (*Mangifera indica* L.). Journal of Agricultural and Food Chemistry, 2003; 51(16): 4527–4531.

[25] Guiamba I R F, Svanberg U, Ahrn´ L. Effect of infrared blanching on enzyme activity and retention of β-carotene and vitamin c in dried mango. Journal of Food Science, 2015; 80(6): E1235–E1242.

[26] Bootkote P, Soponronnarit S, Prachayawarakorn S. Process of producing parboiled rice with different colors by fluidized bed drying technique including tempering. Food Bioprocess Technology, 2016; 9: 1574–1586.

[27] Ju H Y, Vidyarthi S K, Karim M A, Yu X L, Zhang W P, Xiao H W. Drying quality and energy consumption efficient improvements in hot air drying of papaya slices by step-down relative humidity based on heat and mass transfer characteristics and 3D simulation. Drying Technology, 2022; 41(3): 460–476.

[28] Paengkanya S, Soponronnarit S, Nathakaranakule A. Application of microwaves for drying of durian chips. Food and Bioproducts Processing, 2015; 96: 1–11.

[29] Huang Y, Wang X Y, Lyu Y, Li Y, He R R, Chen H M. Metabolomics analysis reveals the non-enzymatic browning mechanism of green peppers (*Piper nigrum* L.) during the hot-air drying process. Food Chemistry, 2025; 464: 141654.

[30] Jiang D-L, Wang Q-H, Huang C, Sutar P P, Lin Y-W, Okaiyeto S A, et al. Effect of various different pretreatment methods on infrared combined hot air impingement drying behavior and physicochemical properties of strawberry slices. Food Chemistry: X, 2024; 22: 101299.

[31] Xu M-Q, Ha B-E, Vidyarthi S K, Zhang F-L, Yang F, Jiang Y-H, et al. Innovative far-infrared radiation assisted pulsed vacuum freeze-drying of banana slices: Drying behaviors, physicochemical properties and microstructural evolution. Innovative Food Science & Emerging Technologies, 2025; 100: 103925.

[32] Cao Y X, Yao X D, Zang Y Z, Niu Y B, Xiao H W, Liu H, et al. Real-time monitoring system for quality monitoring of jujube slice during drying process. Int J Agric & Biol Eng, 2022; 15(3): 234–241.

[33] Jiang D L, Lin Z F, Wu Y T, Pei H J, Li C C. Effects of pulsation ratio on center temperature and drying characteristics of pineapple slices with pulsed vacuum drying. Int J Agric & Biol Eng, 2022; 15(6): 242–253.

[34] Xu H H, Wu M, Zhang T, Gao F, Zheng Z A, Li Y. Effects of different pulsed vacuum drying strategies on drying kinetics, phenolic composition, and antioxidant capacity of chrysanthemum (Imperial chrysanthemum). Int J Agric & Biol Eng, 2022; 15(4): 236–242.

[35] Jiang D L, Shirkole S S, Ju H Y, Niu X X, Xie Y K, Li X Y, et al. An improved infrared combined hot air dryer design and effective drying strategy analysis for sweet potato. LWT-Food Science and Technology, 2025; 215: 117204.

[36] Guo Y T, Wu B G, Guo X Y, Ding F F, Pan Z L, Ma H L. Effects of power ultrasound enhancement on infrared drying of carrot slices: moisture migration and quality characterizations. LWT-Food Science and Technology, 2020; 126: 109312.

[37] Jiang D L, Li C C, Zielinska S, Liu Y H, Gao Z J, Wang R Y, et al. Process performance and quality attributes of temperature and step-down relative humidity controlled hot air drying of Panax notoginseng roots. Int J Agric & Biol Eng, 2021; 14(6): 244–257.

[38] Li B R, Lin J Y, Zheng Z A, Duan H, Li D, Wu M. Effects of different drying methods on drying kinetics and physicochemical properties of Chrysanthemum morifolium Ramat. Int J Agric & Biol Eng, 2019; 12(3): 187–193.

[39] Nimmol C, Devahastin S, Swasdisevi T, Soponronnarit S. Drying of banana slices using combined low-pressure superheated steam and far-infrared radiation. Journal of Food Engineering, 2007; 81: 624–633.

[40] Soponronnarit S, Wetchacama S, Trutassanawin S, Jariyatontivait W. Design, testing, and optimization of vibro-fluidized bed paddy dryer. Drying Technology, 2001; 19(8): 1891–1908.

[41] Soponronnarit S, Prachayawarakorn S. Optimum strategy for fluidized bed paddy drying. Drying Technology, 1994; 12(7): 1667–1686. doi: 0.1080/07373939408962192.

[42] Kitron Y, Tamir A. Performance of a coaxial gas-solid two-impinging-streams (TIS) reactor: Hydrodynamics, residence time distribution, and drying heat transfer. Industrial and Engineering Chemistry Research, 1988; 27: 1760–1767.